Comparison of amniotic membrane versus the induced membrane for bone regeneration in long bone segmental defects using calcium phosphate cement loaded with BMP-2.

Mathilde Fenelon, Marion Etchebarne, Robin Siadous, Agathe Grémare, Marlène Durand, Loic Sentilhes, Sylvain Catros, Florelle Gindraux, Nicolas L'Heureux, Jean-Christophe Fricain

Comparison of amniotic membrane *versus* the induced membrane for bone regeneration in long bone segmental defects using calcium phosphate cement loaded with BMP-2

Mathilde Fénelon*[1,2] Marion Etchebarne[1,3], Robin Siadous[1], Agathe Grémare[1,4], Marlène Durand[1,5,6], Loic Sentilhes[7], Sylvain Catros[1,2], Florelle Gindraux[8,9], Nicolas L'Heureux[1], Jean-Christophe Fricain[1,2]

[1] Univ. Bordeaux, INSERM, BIOTIS, U1026, F-33000 Bordeaux, France

[2] CHU Bordeaux, Department of Oral Surgery, F-33076 Bordeaux, France

[3] CHU Bordeaux, Department of maxillofacial surgery, F-33076 Bordeaux, France

[4] CHU Bordeaux, Odontology and oral health department, F-33076 Bordeaux, France

[5] CHU Bordeaux, CIC 1401, 33000, Bordeaux, France

[6] Inserm, CIC 1401, 33000 Bordeaux, France

[7] CHU Bordeaux, Department of Obstetrics and Gynecology, F-33076, Bordeaux, France

[8] Orthopedic, Traumatology & Plastic Surgery Department - University Hospital of Besançon, Besançon, France

[9] Nanomedicine Lab, Imagery and Therapeutics (EA 4662) - SFR FED 4234 - University of Franche-Comté - Besançon, France

*Corresponding author

mathilde.fenelon@u-bordeaux.fr

ABSTRACT

Thanks to its biological properties, the human amniotic membrane (HAM) combined with a bone substitute could be a single-step surgical alternative to the two-step Masquelet induced membrane (IM) technique for regeneration of critical bone defects. However, no study has directly compared these two membranes.

We first designed a 3D-printed scaffold using calcium phosphate cement (CPC). We assessed its suitability *in vitro* to support human bone marrow mesenchymal stromal cells (hBMSCs) attachment and osteodifferentiation. We then performed a rat femoral critical size defect to compare the two-step IM technique with a single-step approach using the HAM. Five conditions were compared. Group 1 was left empty. Group 2 received the CPC scaffold loaded with rh-BMP2 (CPC/BMP2). Group 3 and 4 received the CPC/BMP2 scaffold covered with lyophilized or decellularized/lyophilized HAM. Group 5 underwent a two- step induced membrane procedure with insertion of a polymethylmethacrylate (PMMA) spacer followed by, after 4 weeks, its replacement with the CPC/BMP2 scaffold wrapped in the IM. Micro-CT and histomorphometric analysis were performed after six weeks.

Results showed that the CPC scaffold supported the proliferation and osteodifferentiation of hBMSCs *in vitro*. *In vivo*, the CPC/BMP2 scaffold very efficiently induced bone formation and led to satisfactory healing of the femoral defect, in a single-step, without autograft or the need for any membrane covering. In this study, there was no difference between the two-step induced membrane procedure and a single step approach. However, the results indicated that none of the tested membranes further enhanced bone healing compared to the CPC/BMP2 group.

Key words: Amniotic membrane; Masquelet induced membrane technique; Bone; 3D-printing; Tissue engineering; Bone morphogenetic protein;

1. INTRODUCTION

The Masquelet technique also called the induced membrane (IM) technique is one of the most commonly used and well-established method to manage critical-sized long bone defects [1–3]. It is a two-step surgical procedure. First, the segmental defect is debrided, the bone is usually stabilized with a plate and a polymethylmethacrylate (PMMA) cement spacer is inserted into the defect [2,3]. This spacer will induce a foreign body reaction thereby leading to the formation of a biological membrane (i.e. the IM) [1]. The second stage is performed six to eight weeks later [2,4]. After carefully removed the spacer, the cavity is filled with cancellous bone autograft from the iliac crest [2]. The IM technique has the benefit of creating an isolated compartment that will protect the bone graft from resorption and invasion by fibrous tissue. It might also be a source of mesenchymal stromal cells or blood vessels and produce osteoinductive growth factors [5–7].

However, the IM technique has some important limitations. The traditional technique involves large quantities of autograft, which can be associated with significant donor site morbidity. Furthermore, the two surgeries required create significant discomfort and risk to the patient as well as additional cost [4]. To overcome these drawbacks, alternatives to the IM technique have been suggested such as using exclusively bone substitutes (avoiding donor site morbidity) and/or using synthetic resorbable membrane (avoiding the first surgical procedure to induce membrane formation) [8–12]. Calcium phosphate-based materials are popular bone substitutes [13,14]. To enhance regeneration in large segmental defect, they usually require growth factors such as bone morphogenetic proteins (BMP). In this study, BMP-2 was chosen for its ability to induce differentiation of osteoprogenitor cells into osteoblasts and to stimulate the formation of new bone [15].

There is still no consensus in the literature regarding the osteoinductive property of the IM [16–18]. It has been indeed suggested that the IM may not have an osteoinductive effect but

only acts as a physical barrier to prevent fibrous tissue ingrowth, according to the concept of guided bone regeneration (GBR) [16,19]. The replacement of the IM by a synthetic membrane has thus been proposed to allow a single-stage procedure, which would remove the additional time needed for IM formation as well as avoid the cost and morbidity of a second surgery. Two studies reported the use of synthetic membranes (polycaprolactone and polytetrafluoroethylene) to cover segmental defects. Tarchala *et al.* observed similar results between a polytetrafluoroethylene membrane and the IM technique [19], whereas the IM promoted greater bone regeneration than a polycaprolactone membrane [9]. Apparently, these membranes clearly only acted as a physical barrier without providing any additional biological effects. Another proposed alternative to avoid an additional surgery was to use polylactic-co-glycolic acid nanofibers as a biodegradable material to replace the PMMA spacer to induce the membrane. Unfortunately, this approach was not directly compared to the IM technique [20].

Thanks to its biological properties, human amniotic membrane (HAM) has become an attractive biological tissue to act as a bioactive membrane for GBR [21–26]. HAM is a readily available biomaterial, derived from human placenta, without ethical concerns. HAM is a source of growth factors [27], and it is also known to possess low immunogenicity [28] and an anti-cancer effect [29]. HAM has been used for over a century for wound healing in medicine [30–33]. However, only a few studies have reported promising results using HAM in the field of orthopedic surgery, and especially, its potential to be used as an alternative to the IM [34–36]. Similarities between the HAM and IM have been shown: both biological membranes are a highly-organized tissue, share similar proteins components and have comparable thicknesses [35]. They both contain growth factors such as VEGF or TGF-β1 and express anti-inflammatory proteins [5,35,37,38]. Finally, some authors reported the

osteogenic capacities of HAM [24,39–41]. Taken together, these findings suggest that HAM could replace the IM and allow a single surgical procedure.

Although the use of amniotic membrane has already been suggested as an alternative to the IM technique, these two membranes have never been directly compared. The objectives of this study were to: 1) design and fabricate a 3D custom scaffold made of osteoconductive calcium phosphate used to replace autologous bone graft in the two-stage IM method and, 2) compare the bone regeneration potential of HAM *versus* that of the IM when they cover this scaffold loaded with BMP-2.

1. Materials and methods

1.1. Materials

1.1.1. 3D Plotting of the bone substitute and post-processing

The bone scaffolds were fabricated using calcium phosphate cements (CPC) paste (InnoTERE® GmbH, Radebeul, Germany). The powder component consisted of 60 wt % a-TCP, 26 wt % calcium hydrogen phosphate, 10 wt % calcium carbonate and 4 wt % precipitated HA [42]. They were fabricated by pressure-assisted micro-extrusion using a dedicated 3D-printer (3D Discovery®, RegenHU, Switzerland). The following plotting parameters were used: needle diameter = 250 µm; plotting speed = 4 $mm.s^{-1}$; dosing pressure = 0,25 MPa.

Two types of scaffolds were fabricated. Circular-shaped scaffolds were used for the *in vitro* characterization experiments. They were plotted in 60° configuration (each layer orientation varied by 60°), provided a triangular inner structure, and a size of 9 mm diameter and 1 mm thick. For the *in vivo* experiments, the scaffold was designed in order to be adjusted into a critical-size rat femoral defect [42]: they were shaped with a cylindrical outer geometry with a height of 5 mm and a diameter of 4 mm and the same triangular inner structure. One side was flattened to allow fixation onto the osteosynthesis plate [42]. Inside each layer and for both

scaffolds, porosity was set at 500 µm. After plotting, the scaffolds were incubated in water-saturated atmosphere at 37°C for 3 days for cement setting, before being sterilized by gamma radiation at 25 kGy (Gamacell® 3000 Elan, NORION MDS, Ottawa, Canada).

1.1.2. Preparation and storage of HAMs

Two treatments of HAM were assessed: lyophilized (L-HAM) and decellularized then lyophilized HAM (DL-HAM). They were prepared as previously described [43]. Two human placentas were collected after elective cesarean surgery from consenting healthy mothers (tested seronegative for HIV, Hepatitis B and C virus, and syphilis). Patients provided written informed consent as requested by the institutional review board and their placentas were anonymized. The placentas were kept in a sterile solution containing PBS 1x (Gibco®) supplemented with 1% antibiotics (penicillin/ streptomycin, Invitrogen®) and transferred to the laboratory. Residual blood clots were removed and the HAM was peeled from the chorion then rinsed with sterile distilled water. All these steps were performed under sterile conditions. To realize lyophilized HAM (L-HAM), patches were frozen at -80°C, then dried under vacuum in a freeze dryer. The decellularization of HAM was performed according to a previously established protocol [43]. Briefly, HAM was first treated with trypsin and ethylenediaminetetraacetic acid (T/EDTA, 0.125%) for two minutes at 37°C. After washing HAM with sterile PBS, HAM was transferred to a decellularization solution composed of 8 mM CHAPS, 25 mM EDTA, 0.12 M NaOH and 1 M NaCl in PBS and incubated, for 7h at room temperature under gentle agitation followed by three washes of sterile distilled water. Finally, DL-HAM was frozen at -80°C then dried in the freeze dryer. L-HAM and DL-HAM were sterilized by gamma radiation at 25 kGy and kept at room temperature.

1.1.3. Preparation of spacers

The bone cement spacers (5mm in length, 5 mm in diameter) were made of polymethyl methacrylate (PMMA) of medical grade (CMW 3, DePuy International, Blackpool, England)

and hardened in silicone moulds (Putty soft, Gumar^{TM,} Acteon®). They were sterilized by gamma radiation at 25 kGy.

1.1.4. BMP-2 solution

A commercially available kit (InductOs®, Medtronic, Biopharma B.V., Heerlen, Netherlands) was used to prepare the solution of rhBMP-2 following the manufacturer's protocol. Prior their implantation *in vivo*, the CPC scaffolds were loaded with a solution containing 10 µg of rhBMP-2: CPC/BMP2.

1.2. *In vitro* evaluation of the cytocompatibility of the scaffolds

In vitro viability and osteogenic differentiation of human bone marrow mesenchymal stem cells (hBMSCs) cultured over the bone substitute were assessed. After getting patient written consent, the hBMSCs were isolated from patients who underwent hip surgery (experimental agreement with *CHU de Bordeaux* and *Etablissement Français du Sang*, agreement CPIS 14.14), and expanded following well-established protocols [44]. Cells were used at passage 2. Then, the circular-shaped scaffolds (9 mm diameter; 1mm height) were put in 48-well plates previously covered by agarose 2 %.

For the viability assay, hBMSCs were seeded onto the CPC scaffolds at a density of 10 x10^4 cells per scaffold and they were cultured in 1 ml of two different mediums: 1) basal medium (BM= α-minimum essential medium (MEM alpha, GIBCO®), 10% fetal bovine serum (Eurobio®) or 2) osteogenic medium (OM= standard osteogenic induction medium (StemPro^{TM}, GIBCO®)). Plates were then incubated at 37°C in a humidified atmosphere containing 5% CO_2 in air. The hBMSCs cultured on tissue culture polystyrene plates served as a positive control.

A live/dead viability assay (Thermo Fisher Scientific, Invitrogen) was performed according to the manufacturer's instructions 3, 7 and 14 days after culture (n=2 per condition and per

time). The staining was visualized with a confocal microscope (Leica TCS SPE Model DMI 4000B).

Qualitative assessment of hBMSCs osteodifferentiation using ALP activity was performed after 7 and 14 days of culture (n=2 per condition and per time). The samples were fixed with 4% paraformaldehyde for 15 min, then washed twice with PBS 1x and processed using the Alkaline Phosphatase kit 86 C-1KT (Sigma-Aldrich, USA) according to the manufacturer's instructions. Briefly, cell layers were incubated with Fast Blue RR salt and Naphtol AS-MX Phosphate Alkaline solution 0.25% (Sigma-Aldrich, USA) for 30 min at room temperature in the dark before being washed in distilled water. Images were obtained using a stereo microscope (MZ10F, Leica Microsystems, Germany) coupled to a camera (Leica model DFC 450C).

1.3. In vivo surgical implantation

1.3.1. Animal model and implantation procedure

The present study was approved by the French Ethics Committee for animal care and experiment (agreement APAFIS n°12543-201712121537848v3). The aim was to compare bone regeneration using L-HAM or DL-HAM, to the IM technique using a femoral critical-size defect model. Fifteen 10-weeks-old male Sprague Dawley rats were used and the surgery was performed on both femurs. They were divided into the following five groups (n=6 per group) (Table 1):

1) Empty group: defects were left empty (**EMPTY**)
2) Control group: defects were filled by the rh-BMP2 loaded calcium phosphate cements (**CPC/BMP2**)
3) The L-HAM group: defects were filled by the CPC/BMP2, then covered by the L-HAM (**L-HAM**)

4) The DL-HAM group: defects were filled by the CPC/BMP2 and covered by the DL-HAM (**DL-HAM**)
5) The IM group: underwent a two-stage procedure with insertion of a PMMA spacer followed by its replacement with the CPC/BMP2 wrapped in the IM (**IM**)

A single step surgical procedure was used for groups 1 to 4, whereas a two-steps surgical procedure was used for group 5. Surgery was carried out under aseptic conditions. Short-term anesthesia was induced by inhalation of 4% isoflurane (Air:1.5 L/min) and maintained using isoflurane 2% (Air: 0.4 L/min). Analgesia was performed by intraperitoneal injection of 0.1 mg/kg buprenorphine (Buprecare®, 0.3 mg/ ml) and rats were given a subcutaneous injection of cephalosporin (cefazoline 0.06mg/kg). The surgical site was aseptically prepared, and a longitudinal 3-cm skin incision was performed laterally across the leg. Dissection of the muscles was performed to expose the femoral shaft. The RatFix™System (RISystem AG, Davos, Switzerland) was mounted to perform standardized 5 mm defect (Fig. 1). Briefly, the osteosynthesis system consisting of a PEEK plate of 23 mm, mounted in the rat femur by six screws, facilitating the placement of the saw guide. Subsequently, two osteotomies were created using a Gigli saw (Fig 1A) and the central mid-diaphyseal bone fragment was removed (Fig 1B). A medial cerclage-wiring technique was performed to ensure enough stability over time. Group 1 defects were left empty for 6 weeks. For groups 2 to 4 the defect was either filled with CCP/BMP2 alone (Fig 1C), or the CCP/BMP-2 was covered by a HAM (Fig 1D) for 6 weeks. Group 5 received an initial PMMA spacer for 4 weeks (Fig 1E), after which the site was reopened to expose the induced membrane created (Fig 1F). After a slight incision through the IM (Fig 1G), the spacer was removed and replaced by the CPC/BMP2 scaffold (Fig 1H) for 6 weeks. The incision made through the IM was closed with absorbable sutures (Vicryl™ 5.0, Ethicon). Finally, the muscles and the superficial fascia were closed using absorbable sutures (Vicryl™ 4.0, Ethicon). The skin was closed with Michel staples and

then covered with aluminum spray (Aluspray®, Vetoquinol, Lure, France). Injection of buprenorphine and cephalosporin were performed the following day after the surgery. Rats were monitored daily for the occurrence of abnormal behavior or complications. At the final time points, the animals were euthanized using CO_2 inhalation. The femurs were dissected and fixed in 4% paraformaldehyde overnight, before being stored into 70% ethanol at 4°C.

1.3.2. Planar X-Rays

After anesthetizing the animals with isoflurane, X-Ray Radiographs were taken immediately after the surgery (Day 0) and every two weeks using Faxitron X-Ray MX20-DC2 digital imaging instrument (Faxitron Bioptics, Arizona, USA). The percentage of bone formation was scored according to a previously described system [12,45] every two weeks post-implantation. We have used a 4-points system. A score of "1" represented 0 to 25 % bone healing, "2" represented 26 to 50 % healing, "3" represented 51 to 75 % healing and "4" represented 76 to 100 % bone healing. The degree of union between the bone substitute and each edge of the defect was also assessed, according to a modified score described previously: 0 = no union, 1 = partial union, 2 = complete radiographical union [46].

1.3.3. Micro-computed tomography

The X-ray microtomographic device used in this study was a Skyscan 1276 (Bruker, Konitch, Belgium). The X-ray source was set at 100 kV and 150 µA to obtain a 15 µm resolution with an exposure time of 450 ms. After scanning, cross-sectional slices were reconstructed using NRecon® reconstruction software (Micro Photonics) and three-dimensional analysis was performed using CTAn® visualization software (Bruker, Konitch, Belgium). A volume of interest of 5 mm length and 333-slice thickness was determined for each femur and applied to all reconstructions. Bone volume fraction (bone volume/total volume [BV/TV]) was assessed.

1.3.4. Histological preparation and histomorphometric analysis

Each sample was decalcified with EDTA-based Microdec® decalcifiant for 3 weeks. The samples were dehydrated and processed for conventional embedding in paraffin. Eight-µm-thick serial sections were prepared through the middle of the defect and stained with Masson's trichrome and HES staining. Images of the 30 samples stained with Masson's trichrome staining were obtained with an Eclipse 80i light microscope (Nikon, Japan) and captured with a DXM 1200C CCD camera (Nikon, Japan). Morphometric analysis was performed using ImageJ® software for each femoral specimen to quantify the percentage of bone formation inside the pores of each scaffold for group 2 to 5. A previously described histological quantitative scoring system [12] was also used to evaluate the tissue response around the scaffold surface and within the pores (Table 2). Finally, samples stained with HES were acquired with a slide scanner (Hamamatsu Nanozoomer 2.0HT) and a quantitative analysis of blood vessels within the pores of the CPC scaffold was performed using NDPview software. Blood vessels were identified by their luminal structure and the presence of red blood cells within their boundaries. Blood vessel density (BVD) was determined by the number of new blood vessels in the scaffold divided by the entire scaffold area [47–49].

1.4. Statistical analysis

Results were expressed as mean ± standard deviation (SD), with n indicating the number of HAM sample tested. Statistical analysis was performed using GraphPad Prism® Software (La Jolla/CA, USA). First, normality test was performed using a D'Agostino and Pearson omnibus normality test. Statistical significance for independent samples was evaluated with the non-parametric Kruskal-Wallis test followed by Dunn's multiple comparison test. In all cases, statistical significances are marked by stars with * indicating a two-tailed $p < 0.05$, ** $p < 0.01$, and *** $p < 0.001$.

2. RESULTS

2.1. *In vitro* viability and osteogenic differentiation of hBMSCs cultured on the bone substitute

We assessed the suitability of the bone substitute to be used as a scaffold upon which hBMSCs could survive and differentiate towards the osteogenic lineage. Live/dead staining revealed that hBMSCs attached to and spread over the surface of the plotted CPC scaffolds overtime (Fig 2). At day 14, qualitative observations revealed more cells in the scaffold surface when OM was used. Similar results were observed on standard tissue culture polystyrene.

At the early time-point (day 3), a slight ALP staining of hBMSCs was observed, mainly at the periphery of the scaffold, in both culture media (Fig 3). After seven days, a strong ALP staining of hBMSCs was observed on the scaffold cultured in OM. This intense staining was observed over the entire surface of the scaffold. Similarly, an increase of positive ALP staining was observed when hBMSCs were seeded on plastic in OM compared to BM. This staining appeared less intense than the one observed on the scaffold.

2.2. *In vivo* study

2.2.1. Study population

All 15 rats survived to surgery. The animals were continuously monitored and did not exhibit any signs of pain. We also observed regular feeding habits and normal ambulation from the day after surgery.

2.2.2. Planar X-Rays

Figure 4A shows representative x-ray radiographs for the five groups: 1) defect left empty (EMPTY), 2) filled by the rh-BMP2 loaded calcium phosphate cements (CPC/BMP2), 3) filled by CPC/BMP2 then covered by the lyophilized HAM (L-HAM), 4) filled by CPC/BMP2 then covered by the decellularized/lyophilized HAM (DL-HAM), 5) filled by CPC/BMP2 wrapped in the IM. In all cases, bone formation substantially increased between two and four weeks after the surgery. Six weeks after the surgery, complete or nearly complete healing (defined as a score greater than 3) was observed in groups 2 to 5 (Fig 4B). No ectopic bone formation was observed in surrounding subcutaneous tissues or muscles. The scores resulting from the degree of union showed that bridging between scaffold and bone increased overtime for all conditions (Fig 4C).

2.2.3. Micro-CT analysis

Figure 5A shows representative 3D-reconstruction of the region of interest. Bone volume fraction (BV/TV) within the defect was evaluated quantitatively at 6 weeks (Fig 5B). BV/TV was significantly higher for the following three groups CPC/BMP2, IM and DL-HAM compared to the defect left empty, but neither of these two membranes promoted bone healing compared to the CPC/BMP2 group. Covering the BMP2 loaded bone substitute using L-HAM significantly reduced the BV/TV compared to the DL-HAM group.

2.2.4. Histomorphological analysis

No fibrous encapsulation was observed in response to the scaffold (Fig 6A). Tissues at various stages of bone healing were found in the defect sites, with extensive regeneration of mineralized bone in all groups except for the empty group. Newly formed bone and marrow tissues were found throughout the scaffolds both in direct contact with the scaffold and within the pores.

Histomorphological analysis was performed to quantify bone regeneration inside the pores of the scaffold for groups 2 to 5 (Fig 6B). The nature of the tissue formed inside the pores was mostly bone, and few dense fibrous as well as marrow tissues were also observed. The highest level of bone formation inside pores was observed when the bone substitute was covered by the IM, without significant difference.

To further investigate the tissue response at the interface between the bone and the scaffold and within the pores, a histological tissue response scoring was performed for groups 2 to 5 (Fig 6 C-E). Fig 6C shows tissue response scores at the rod interface. The majority of the samples showed a score greater than or equal to 3 demonstrating a direct bone contact with the scaffold without fibrous tissue encapsulation. Tissue within the pores was mostly bone associated with mature or immature fibrous tissue (Fig 6D). Only the L-HAM group showed some samples where connective tissue was mostly observed inside pores, as demonstrated by a significantly lower scoring of the hard tissue response within the pores compared to the IM group. Fig 6E showed the total tissue response score. The L-HAM group showed the lowest score without statistical significance.

Finally, the vascularization within the pores of the CPC scaffold was assessed from histological sections stained with HES (Fig 7A and B). Newly formed blood vessels were observed within the pores of the scaffold similarly in these conditions (Fig 7C).

DISCUSSION

The aim of this study was to compare, for the first time, the well-established IM method to a single step procedure using DL-HAM or L-HAM for bone regeneration. We also aimed to investigate the ability of the 3D-printed CPC scaffold loaded with rh-BMP2 to promote bone regeneration without autograft harvest in a critical size femoral defect in rats.

One major limitation of the IM technique is the need for a high quantity of autologous bone graft. However, only a few studies have investigated bone substitutes in a Masquelet-inspired animal model using traditional PMMA [9,19]. The layer-by-layer construction of 3D structures allows precise control over the inner architecture and the shape of the scaffold in order to fit a specific defect [42]. The porosity of a scaffold plays a key role for cell migration, vascularization and new bone ingrowth. We choose a calcium phosphate-based biomaterial because these biomaterials are known to increase osteoprogenitors cells and capillaries ingrowth in large bone defects [13,14,50]. We produced inner pores with a triangular cross-section because it affects positively scaffold vascular colonization and its osteointegration [51,52]. *In vitro* results showed that the CPC scaffold allows hBMSCs proliferation when seeded over the scaffold. Furthermore, hBMSCs osteodifferentiation was observed through the entire surface of the scaffold.

The CPC scaffold is an osteoconductive biomaterial which lacks growth factors and living cells found in autologous grafts. We thus loaded the CPC scaffold with 10 µg of rh-BMP-2 to overcome its lack of osteoinductive properties. This dosage is consistent with previous studies of critical-sized femoral defect of 3 to 6 mm in rats [53,54,54–56]. However, further studies would be necessary to assess the release kinetics and the dose-response of BMP-2 on the CPC to improve the system. In our study, nearly complete healing was observed with the CPC scaffold loaded with BMP-2. Histological analysis showed a direct bone contact between the scaffold and the adjacent host bone without fibrous tissue encapsulation. Newly formed bone was also observed within the scaffold pores. In addition, as vascularization of a bone substitute in large bone defect is often challenging [57], we investigated the angiogenesis inside the CPC scaffold. Interestingly, results showed blood vessels formation within the CPC pores, which is necessary to allow bone regeneration. The lack of a BMP-2 control group and of a conventional Masquelet control group are two limitations of this study. Conventional

Masquelet technique required cancellous bone autograft to fill up the cavity. However, it was not possible to harvest such an amount of cancellous bone using this small animal model. In future research, an alternative would be to perform a study in a larger animal model [58–60]. Finally, we did not perform a BMP-2 control group, as well as a CPC control group, as the goal of this study was to compare osseous healing between membrane groups, not to study the BMP-2 or the CPC biomaterial effects.

In clinical practice, PMMA is used as a cement spacer to fill up the bone cavity to induce membrane formation and did not require prior sterilization. In our model, it was not possible to cast the spacer into the defect during surgery. We thus premade PMMA spacers which required to use gamma-radiation to sterilize them prior to surgery as previously described [61]. The lack of information regarding influence of gamma-radiation on the membrane properties as well as on degradation products release is another limitation of this study.

While it is preferable to maintain a two-stage technique in case of infection and septic bone non-union [62], the repair of bone defects following trauma or tumor resection may be performed in a single step. To this end, it has been suggested to replace the induced membrane with a readily available biological membrane to shorten therapy [63]. Similar osseous healing has been observed when using a human acellular dermis, in a one-stage surgery, or the induce membrane for the treatment of non-infectious large bone defects in rats [63]. Here, we decided to evaluate the effect of HAM which is a biological membrane showing similar properties to the induce membrane. It has been shown that F-HAM displays a strong osteogenic potential [41,64] and has a “periosteum effect” when used to cover a segmental long bone defect in rabbits [40]. However, to avoid the risk of infectious disease transmission and to allow long-term storage, HAM cannot be used as a fresh tissue. Cryopreservation, lyophilization or decellularization/lyophilization combined with gamma sterilization, are the most commonly used protocols for HAM preservation [24,65]. We

previously characterized these three membranes and we already demonstrated our decellularization protocol efficiency [43]. We reported that L-HAM degraded faster than DL-HAM, but that they both showed a slower resorption rate than cryopreserved HAM when implanted subcutaneously [43]. We also previously observed that both L- and DL-HAM displayed a higher ability to act as a barrier membrane for GBR in a non-critical size femoral defect in mice than cryopreserved HAM [26]. We thus decided to compare the IM to the L-HAM and DL-HAM. We hypothesized that the presence of the membrane would limit dispersion of the BMP-2 and maintains the growth factor inside the bone defect. However, no additional effect on bone regeneration was achieved by covering the CPC/BMP2 scaffold with the IM or the DL-HAM. Despite the low dose of BMP-2, the barrier membrane effect appears to have been masked by the effect of the growth factor. The association of BMP-2 and a bone substitute to fill a rat segmental defect using a two-step surgical approach has only been investigated in one study [53]. Interestingly, they observed a significant higher level of bone formation when they performed a debridement of the IM before filling the defect, therefore suggesting an inhibition of the effect of BMP-2 by the IM. One preclinical study investigated bone regeneration using a calcium phosphate scaffold loaded with BMP-2 covered or not with three different barrier membranes in a rabbit calvarial model. They also observed no beneficial effect of barrier membranes on bone regeneration [13]. This would suggest an inhibitory activity between the added rhBMP-2 and growth factors contained in both the IM and the HAM such as TGF-β1 [5,35]. Indeed, the opposite effects between TGF-β1 and BMP-2 on osteoblast differentiation and maturation have been previously reported [66]. This hypothesis would be consistent with our previous study, in which we observed no additional benefit when using cryopreserved HAM to cover a calvarial defect filled by a bone substitute and BMP-2 in mice [21]. Finally, Masquelet *et al.* also reported no additional effect of the IM when associated with BMP-7, which is another osteoinductive growth factor [2].

After removing the spacer during the second surgery, they filled the IM space with bone autograft mixed with rhBMP-7 in eleven patients. The authors concluded that the results of this case-series were not improved compared with the conventional technique. It could thus be interesting to perform the same study without BMP-2 so we might observe a membrane effect.

To our knowledge, the decellularized HAM had never been evaluated in a segmental bone defect model. In this study, results highlighted a negative effect of L-HAM on total bone volume formation and on bone formation within the pores of the CPC scaffold (Fig 5 B and fig 6 D) thereby suggesting that the DL-HAM is the most suitable preserved HAM to be compared with the IM. This could be explained by the higher ability of DL-HAM to promote hBMSCs proliferation and to support their osteodifferentiation compared to L-HAM [26]. Moreover, bone healing required several weeks and we previously reported that DL-HAM had a superior persistence *in vivo* [43], thereby preventing the invasion of fibrous tissue over a longer period. Few studies have previously reported promising results achieved with a decellularized HAM for non-critical bone regeneration [24,67].

CONCLUSION

In conclusion, the CPC/BMP2 scaffold very efficiently induced bone formation and led to satisfactory healing of the femoral defect at 6 weeks, in a single-step, without autograft or the need for any membrane covering. In this study, there was no difference between the two-step Masquelet approach and a single step approach. However, the results showed that none of the tested membranes further enhanced bone healing compared to the CPC/BMP2 group.

FIGURE LEGENDS

Figure 1. Surgical protocol. (A) Two osteotomies were created using a Gigli saw and the saw guide, (B) the central mid-diaphyseal bone fragment was removed and (C) replaced with the CPC scaffold, (D) before being covered by the HAM. The two steps-protocol consisted of (E) the surgical implantation of the PMMA spacer in the bone defect, followed by the subsequent (F) formation of the induced membrane four weeks later (G) which was incised to remove the spacer and (H) replace it with the CPC scaffold wrapped in the induced membrane. Black arrowhead : CPC scaffold ;White arrow: HAM; Blue asterix: PMMA spacer; Yellow arrow: Induced membrane. (I) Bone fragment and CPC scaffold.

Figure 2. *In vitro* cell viability assays. Fluorescence micrographs of hBMSCs cultured on 3D-printed CPC based bone substitute or standard culture polystyrene (control). Living cells (green) attached and proliferated well on the synthetic scaffold. Dead cells (red) were rarely observed. BM: Basal medium; OM: Osteogenic medium. Scale bar: 100µm.

Figure 3. *In vitro* osteodifferentiation. Alcaline phosphatase staining (blue) was performed to assess the ability of hBMSCs to osteodifferentiate when seeded on the CPC scaffold or on tissue culture plates (control).

Figure 4. **Longitudinal X-Rays follow-up.** (A) Representative 2D-radiographs showing the segmental defect immediately after the surgery as well as 2, 4 and 6 weeks after the surgery. Radiographic scoring was performed to quantify (B) bone formation in the 5 groups and (C) the degree of union between the CPC scaffold and the bone. Data are presented as means ± SD; n=6 per condition and per time; * $p < 0.05$, ** $p < 0.01$.

Figure 5. **Micro-CT analysis.** (A) Representative 3D rendering showing the region of interest at six weeks. (B) Quantitative analysis was performed for bone regeneration (BV/TV(%)). Data are presented as means ± SD; n=6 per condition; * $p<0.05$, ** $p < 0.01$, *** $p<0.001$.

Figure 6. **Histomorphological analysis of bone regeneration.** (A) Representative histological sections stained with Masson trichrome staining at six weeks to visualize mineralized bone (blue). Yellow arrow: newly formed bone; BM: bone marrow; Red line represents the edges of the CPC scaffold inside which bone formation was quantified (B) Quantitative analysis was performed to assess the percentage of bone formation within pores. (C-E) A histological tissue response scoring was performed for groups 2 to 5. Data are presented as means ± SD; n=6 per condition; * $p<0.05$.

Figure 7. Histomorphological analysis of angiogenesis in decalcified femoral defects. (A) Representative histological sections (HES staining) of explanted femoral defect six weeks after the surgery. Scale bar: 1 mm. (B) Higher magnification image of the blue rectangle. Erythrocytes were stained pink and densely organized collagen fibers in orange-pink. NB: new bone; BM: bone marrow; Red line represents the edges of the CPC scaffold inside which the vessels were quantified; Black arrow: new blood vessels; Red arrow: newly formed bone. Asterix: surrounding native bone. Scale bar: **2**50 µm. (C) New blood vessels density. Data are presented as means ± SD, n=6 per condition.

TABLE LEGENDS

Table 1. Description of the five experimental conditions used for the in vivo implantation (n=6 per group).

Table 2. Histological quantitative scoring system.

Acknowledgements:

This work contributes to the COST Action CA17116 "*International Network for Translating Research on Perinatal Derivatives into Therapeutic Approaches (SPRINT)*", supported by COST (European Cooperation in Science and Technology). The authors acknowledge *La Fondation des gueules cassées* for financial support. The authors also thank Dr Vera Guduric

and Dr Tijana Lainović (Medical Faculty, School of Dentistry, University of Novi Sad, Serbia) for their help to design the CPC scaffold, Laetitia Medan as manager of the animal facility, Dr Richard Walton for his expertise and guidance acquiring the microCT data sets and the IHU-Liryc institute (University of Bordeaux, Pessac, France) for access to the scanner, Dr Delphine Maurel (UMR1026 BioTis) for scanner analysis expertise and Patrick Guitton for his technical support. Acquisition of histological (HES) images with the slide scanner was performed in the Bordeaux Imaging Center (a service unit of the CNRS-INSERM and Bordeaux University) with the help of Sébastien Marais.

Conflict of interest: None

BIBLIOGRAPHY

[1] C. Karger, T. Kishi, L. Schneider, F. Fitoussi, A.-C. Masquelet, French Society of Orthopaedic Surgery and Traumatology (SoFCOT), Treatment of posttraumatic bone defects by the induced membrane technique, Orthop. Traumatol. Surg. Res. OTSR. 98 (2012) 97–102. https://doi.org/10.1016/j.otsr.2011.11.001.
[2] A.C. Masquelet, T. Begue, The concept of induced membrane for reconstruction of long bone defects, Orthop. Clin. North Am. 41 (2010) 27–37; table of contents. https://doi.org/10.1016/j.ocl.2009.07.011.
[3] P.V. Giannoudis, O. Faour, T. Goff, N. Kanakaris, R. Dimitriou, Masquelet technique for the treatment of bone defects: tips-tricks and future directions, Injury. 42 (2011) 591–598. https://doi.org/10.1016/j.injury.2011.03.036.
[4] I. Morelli, L. Drago, D.A. George, E. Gallazzi, S. Scarponi, C.L. Romanò, Masquelet technique: myth or reality? A systematic review and meta-analysis, Injury. 47 (2016) S68–S76. https://doi.org/10.1016/S0020-1383(16)30842-7.
[5] P. Pelissier, A.C. Masquelet, R. Bareille, S.M. Pelissier, J. Amedee, Induced membranes secrete growth factors including vascular and osteoinductive factors and could stimulate bone regeneration, J. Orthop. Res. Off. Publ. Orthop. Res. Soc. 22 (2004) 73–79. https://doi.org/10.1016/S0736-0266(03)00165-7.
[6] H.E. Gruber, G. Ode, G. Hoelscher, J. Ingram, S. Bethea, M.J. Bosse, Osteogenic, stem cell and molecular characterisation of the human induced membrane from extremity bone defects, Bone Jt. Res. 5 (2016) 106–115. https://doi.org/10.1302/2046-3758.54.2000483.
[7] F. Gindraux, F. Loisel, M. Bourgeois, K. Oudina, M. Melin, B. de Billy, P. Sergent, G. Leclerc, H. Petite, F. Auber, L. Obert, I. Pluvy, Induced membrane maintains its osteogenic properties even when the second stage of Masquelet's technique is performed later, Eur. J. Trauma Emerg. Surg. Off. Publ. Eur. Trauma Soc. 46 (2020) 301–312. https://doi.org/10.1007/s00068-019-01184-4.
[8] P. Pélissier, Y. Lefevre, S. Delmond, F. Villars, J. Vilamitjana-Amedee, [Influences of induced membranes on heterotopic bone formation within an osteo-inductive complex. Experimental study in rabbits], Ann. Chir. Plast. Esthet. 54 (2009) 16–20. https://doi.org/10.1016/j.anplas.2008.07.001.
[9] M.R. DeBaun, A.M. Stahl, A.I. Daoud, C.-C. Pan, J.A. Bishop, M.J. Gardner, Y.P. Yang, Preclinical induced membrane model to evaluate synthetic implants for healing critical bone defects without autograft, J. Orthop. Res. Off. Publ. Orthop. Res. Soc. (2018). https://doi.org/10.1002/jor.24153.
[10] R. Dimitriou, G.I. Mataliotakis, G.M. Calori, P.V. Giannoudis, The role of barrier membranes for guided bone regeneration and restoration of large bone defects: current experimental and clinical evidence, BMC Med. 10 (2012) 81. https://doi.org/10.1186/1741-7015-10-81.
[11] P. Bosemark, C. Perdikouri, M. Pelkonen, H. Isaksson, M. Tägil, The masquelet induced membrane technique with BMP and a synthetic scaffold can heal a rat femoral critical size defect, J. Orthop. Res. Off. Publ. Orthop. Res. Soc. 33 (2015) 488–495. https://doi.org/10.1002/jor.22815.
[12] A.M. Henslee, P.P. Spicer, D.M. Yoon, M.B. Nair, V.V. Meretoja, K.E. Witherel, J.A. Jansen, A.G. Mikos, F.K. Kasper, Biodegradable composite scaffolds incorporating an intramedullary rod and delivering bone morphogenetic protein-2 for stabilization and bone regeneration in segmental long bone defects, Acta Biomater. 7 (2011) 3627–3637. https://doi.org/10.1016/j.actbio.2011.06.043.
[13] C. Schopper, D. Moser, E. Spassova, W. Goriwoda, G. Lagogiannis, B. Hoering, R. Ewers, H. Redl, Bone regeneration using a naturally grown HA/TCP carrier loaded with rh

BMP-2 is independent of barrier-membrane effects, J. Biomed. Mater. Res. A. 85 (2008) 954–963. https://doi.org/10.1002/jbm.a.31525.
[14] F. Espitalier, C. Vinatier, E. Lerouxel, J. Guicheux, P. Pilet, F. Moreau, G. Daculsi, P. Weiss, O. Malard, A comparison between bone reconstruction following the use of mesenchymal stem cells and total bone marrow in association with calcium phosphate scaffold in irradiated bone, Biomaterials. 30 (2009) 763–769. https://doi.org/10.1016/j.biomaterials.2008.10.051.
[15] M. Szpalski, R. Gunzburg, Recombinant human bone morphogenetic protein-2: a novel osteoinductive alternative to autogenous bone graft?, Acta Orthop. Belg. 71 (2005) 133–148.
[16] S. Catros, N. Zwetyenga, R. Bareille, B. Brouillaud, M. Renard, J. Amédée, J.-C. Fricain, Subcutaneous-induced membranes have no osteoinductive effect on macroporous HA-TCP in vivo, J. Orthop. Res. Off. Publ. Orthop. Res. Soc. 27 (2009) 155–161. https://doi.org/10.1002/jor.20738.
[17] F. Jin, Y. Xie, N. Wang, X. Qu, J. Lu, Y. Hao, K. Dai, Poor osteoinductive potential of subcutaneous bone cement-induced membranes for tissue engineered bone, Connect. Tissue Res. 54 (2013) 283–289. https://doi.org/10.3109/03008207.2013.811499.
[18] D. Henrich, C. Seebach, C. Nau, S. Basan, B. Relja, K. Wilhelm, A. Schaible, J. Frank, J. Barker, I. Marzi, Establishment and characterization of the Masquelet induced membrane technique in a rat femur critical-sized defect model, J. Tissue Eng. Regen. Med. 10 (2016) E382–E396. https://doi.org/10.1002/term.1826.
[19] M. Tarchala, V. Engel, J. Barralet, E.J. Harvey, A pilot study: Alternative biomaterials in critical sized bone defect treatment, Injury. 49 (2018) 523–531. https://doi.org/10.1016/j.injury.2017.11.007.
[20] Y.-H. Yu, R.-C. Wu, D. Lee, C.-K. Chen, S.-J. Liu, Artificial Membrane Induced by Novel Biodegradable Nanofibers in the Masquelet Procedure for Treatment of Segmental Bone Defects, J. Nanomater. 2018 (2018) e8246571. https://doi.org/10.1155/2018/8246571.
[21] M. Fénelon, O. Chassande, J. Kalisky, F. Gindraux, S. Brun, R. Bareille, Z. Ivanovic, J.-C. Fricain, C. Boiziau, Human amniotic membrane for guided bone regeneration of calvarial defects in mice, J. Mater. Sci. Mater. Med. 29 (2018) 78. https://doi.org/10.1007/s10856-018-6086-9.
[22] M.F. Gomes, M.J. dos Anjos, T.O. Nogueira, S.A. Guimarães, Histologic evaluation of the osteoinductive property of autogenous demineralized dentin matrix on surgical bone defects in rabbit skulls using human amniotic membrane for guided bone regeneration, Int. J. Oral Maxillofac. Implants. 16 (2001) 563–571.
[23] S. Koushaei, M.H. Samandari, S.M. Razavi, A. Khoshzaban, S. Adibi, P. Varedi, Histological Comparison of New Bone Formation Using Amnion Membrane Graft vs Resorbable Collagen Membrane: An Animal Study, J. Oral Implantol. (2018). https://doi.org/10.1563/aaid-joi-D-16-00120.
[24] K. Tang, J. Wu, Z. Xiong, Y. Ji, T. Sun, X. Guo, Human acellular amniotic membrane: A potential osteoinductive biomaterial for bone regeneration, J. Biomater. Appl. (2017) 885328217739753. https://doi.org/10.1177/0885328217739753.
[25] F. Akhlaghi, N. Hesami, M.R. Rad, P. Nazeman, F. Fahimipour, A. Khojasteh, Improved bone regeneration through amniotic membrane loaded with buccal fat pad-derived MSCs as an adjuvant in maxillomandibular reconstruction, J. Cranio-Maxillo-Fac. Surg. Off. Publ. Eur. Assoc. Cranio-Maxillo-Fac. Surg. (2019). https://doi.org/10.1016/j.jcms.2019.03.030.
[26] M. Fénelon, M. Etchebarne, R. Siadous, A. Grémare, M. Durand, L. Sentilhes, Y. Torres, S. Catros, F. Gindraux, N. L'Heureux, J.-C. Fricain, Assessment of fresh and preserved amniotic membrane for guided bone regeneration in mice, J. Biomed. Mater. Res.

A. (2020). https://doi.org/10.1002/jbm.a.36964.
[27] N.J. Koizumi, T.J. Inatomi, C.J. Sotozono, N.J. Fullwood, A.J. Quantock, S. Kinoshita, Growth factor mRNA and protein in preserved human amniotic membrane, Curr. Eye Res. 20 (2000) 173–177.
[28] M. Kubo, Y. Sonoda, R. Muramatsu, M. Usui, Immunogenicity of human amniotic membrane in experimental xenotransplantation, Invest. Ophthalmol. Vis. Sci. 42 (2001) 1539–1546.
[29] H. Niknejad, G. Yazdanpanah, Anticancer effects of human amniotic membrane and its epithelial cells, Med. Hypotheses. 82 (2014) 488–489. https://doi.org/10.1016/j.mehy.2014.01.034.
[30] A. Sorsby, J. Haythorne, H. Reed, FURTHER EXPERIENCE WITH AMNIOTIC MEMBRANE GRAFTS IN CAUSTIC BURNS OF THE EYE, Br. J. Ophthalmol. 31 (1947) 409–418. https://doi.org/10.1136/bjo.31.7.409.
[31] W.J. Schrimpf, Repair of tympanic membrane perforations with human amniotic membrane; report of fifty-three cases, Ann. Otol. Rhinol. Laryngol. 63 (1954) 101–115. https://doi.org/10.1177/000348945406300109.
[32] J.S. Davis, II. Skin Grafting at the Johns Hopkins Hospital, Ann. Surg. 50 (1909) 542–549. https://doi.org/10.1097/00000658-190909000-00002.
[33] M. Song, W. Wang, Q. Ye, S. Bu, Z. Shen, Y. Zhu, The repairing of full-thickness skin deficiency and its biological mechanism using decellularized human amniotic membrane as the wound dressing, Mater. Sci. Eng. C Mater. Biol. Appl. 77 (2017) 739–747. https://doi.org/10.1016/j.msec.2017.03.232.
[34] Moosavi S S, Fakoor M, Abbaszadeh A, Ghasemi M A, Ranjbari N, Hoseini P M, Sadooni H, Evaluation of Osteoinductive and Osteoconductive Effect of the Amniotic Membrane in Bone Defects due to Open Fractures in Rabbits, J Orthop Spine Trauma. (2018). https://doi.org/10.5812/jost.77154.
[35] F. Gindraux, T. Rondot, B. de Billy, N. Zwetyenga, J.-C. Fricain, A. Pagnon, L. Obert, Similarities between induced membrane and amniotic membrane: Novelty for bone repair, Placenta. (2017). https://doi.org/10.1016/j.placenta.2017.06.340.
[36] N. Heckmann, R. Auran, R. Mirzayan, Application of Amniotic Tissue in Orthopedic Surgery, Am. J. Orthop. Belle Mead NJ. 45 (2016) E421–E425.
[37] Z. Grzywocz, E. Pius-Sadowska, P. Klos, M. Gryzik, D. Wasilewska, B. Aleksandrowicz, M. Dworczynska, S. Sabalinska, G. Hoser, B. Machalinski, J. Kawiak, Growth factors and their receptors derived from human amniotic cells in vitro, Folia Histochem. Cytobiol. Pol. Acad. Sci. Pol. Histochem. Cytochem. Soc. 52 (2014) 163–170. https://doi.org/10.5603/FHC.2014.0019.
[38] M. Litwiniuk, M. Radowicka, A. Krejner, A. Śladowska, T. Grzela, Amount and distribution of selected biologically active factors in amniotic membrane depends on the part of amnion and mode of childbirth. Can we predict properties of amnion dressing? A proof-of-concept study, Cent.-Eur. J. Immunol. 43 (2018) 97–102. https://doi.org/10.5114/ceji.2017.69632.
[39] Y.-J. Chen, M.-C. Chung, C.-C. Jane Yao, C.-H. Huang, H.-H. Chang, J.-H. Jeng, T.-H. Young, The effects of acellular amniotic membrane matrix on osteogenic differentiation and ERK1/2 signaling in human dental apical papilla cells, Biomaterials. 33 (2012) 455–463. https://doi.org/10.1016/j.biomaterials.2011.09.065.
[40] S. Ghanmi, M. Trigui, W. Baya, Z. Ellouz, A. Elfeki, S. Charfi, J.C. Fricain, H. Keskes, The periosteum-like effect of fresh human amniotic membrane on bone regeneration in a rabbit critical-sized defect model, Bone. 110 (2018) 392–404. https://doi.org/10.1016/j.bone.2018.03.004.
[41] A. Lindenmair, S. Wolbank, G. Stadler, A. Meinl, A. Peterbauer-Scherb, J. Eibl, H.

Polin, C. Gabriel, M. van Griensven, H. Redl, Osteogenic differentiation of intact human amniotic membrane, Biomaterials. 31 (2010) 8659–8665. https://doi.org/10.1016/j.biomaterials.2010.07.090.
[42] T. Ahlfeld, A.R. Akkineni, Y. Förster, T. Köhler, S. Knaack, M. Gelinsky, A. Lode, Design and Fabrication of Complex Scaffolds for Bone Defect Healing: Combined 3D Plotting of a Calcium Phosphate Cement and a Growth Factor-Loaded Hydrogel, Ann. Biomed. Eng. 45 (2017) 224–236. https://doi.org/10.1007/s10439-016-1685-4.
[43] M. Fenelon, D. B Maurel, R. Siadous, A. Gremare, S. Delmond, M. Durand, S. Brun, S. Catros, F. Gindraux, N. L'Heureux, J.-C. Fricain, Comparison of the impact of preservation methods on amniotic membrane properties for tissue engineering applications, Mater. Sci. Eng. C. 104 (2019) 109903. https://doi.org/10.1016/j.msec.2019.109903.
[44] J. Vilamitjana-Amedee, R. Bareille, F. Rouais, A.I. Caplan, M.F. Harmand, Human bone marrow stromal cells express an osteoblastic phenotype in culture, In Vitro Cell. Dev. Biol. Anim. 29A (1993) 699–707.
[45] E.L. Hedberg, H.C. Kroese-Deutman, C.K. Shih, J.J. Lemoine, M.A.K. Liebschner, M.J. Miller, A.W. Yasko, R.S. Crowther, D.H. Carney, A.G. Mikos, J.A. Jansen, Methods: a comparative analysis of radiography, microcomputed tomography, and histology for bone tissue engineering, Tissue Eng. 11 (2005) 1356–1367. https://doi.org/10.1089/ten.2005.11.1356.
[46] V.M. Goldberg, A. Powell, J.W. Shaffer, J. Zika, G.D. Bos, K.G. Heiple, Bone grafting: role of histocompatibility in transplantation, J. Orthop. Res. Off. Publ. Orthop. Res. Soc. 3 (1985) 389–404. https://doi.org/10.1002/jor.1100030401.
[47] W. Chen, J. Liu, N. Manuchehrabadi, M.D. Weir, Z. Zhu, H.H.K. Xu, Umbilical cord and bone marrow mesenchymal stem cell seeding on macroporous calcium phosphate for bone regeneration in rat cranial defects, Biomaterials. 34 (2013) 9917–9925. https://doi.org/10.1016/j.biomaterials.2013.09.002.
[48] P. Wang, L. Zhao, W. Chen, X. Liu, M.D. Weir, H.H.K. Xu, Stem Cells and Calcium Phosphate Cement Scaffolds for Bone Regeneration, J. Dent. Res. 93 (2014) 618–625. https://doi.org/10.1177/0022034514534689.
[49] X. Liu, P. Wang, W. Chen, M.D. Weir, C. Bao, H.H.K. Xu, Human embryonic stem cells and macroporous calcium phosphate construct for bone regeneration in cranial defects in rats, Acta Biomater. 10 (2014) 4484–4493. https://doi.org/10.1016/j.actbio.2014.06.027.
[50] T. Yoshii, S. Sotome, I. Torigoe, A. Tsuchiya, H. Maehara, S. Ichinose, K. Shinomiya, Fresh bone marrow introduction into porous scaffolds using a simple low-pressure loading method for effective osteogenesis in a rabbit model, J. Orthop. Res. Off. Publ. Orthop. Res. Soc. 27 (2009) 1–7. https://doi.org/10.1002/jor.20630.
[51] A. Magnaudeix, J. Usseglio, M. Lasgorceix, F. Lalloue, C. Damia, J. Brie, P. Pascaud-Mathieu, E. Champion, Quantitative analysis of vascular colonisation and angio-conduction in porous silicon-substituted hydroxyapatite with various pore shapes in a chick chorioallantoic membrane (CAM) model, Acta Biomater. 38 (2016) 179–189. https://doi.org/10.1016/j.actbio.2016.04.039.
[52] S. Van Bael, Y.C. Chai, S. Truscello, M. Moesen, G. Kerckhofs, H. Van Oosterwyck, J.-P. Kruth, J. Schrooten, The effect of pore geometry on the in vitro biological behavior of human periosteum-derived cells seeded on selective laser-melted Ti6Al4V bone scaffolds, Acta Biomater. 8 (2012) 2824–2834. https://doi.org/10.1016/j.actbio.2012.04.001.
[53] S. Schützenberger, M. Kaipel, A. Schultz, T. Nau, H. Redl, T. Hausner, Non-union site debridement increased the efficacy of rhBMP-2 in a rodent model, Injury. 45 (2014) 1165–1170. https://doi.org/10.1016/j.injury.2014.05.004.
[54] Y. Morishita, M. Naito, M. Miyazaki, W. He, G. Wu, F. Wei, C. Sintuu, H. Hymanson, E.J. Brochmann, S.S. Murray, J.C. Wang, Enhanced effects of BMP-binding

peptide combined with recombinant human BMP-2 on the healing of a rodent segmental femoral defect, J. Orthop. Res. Off. Publ. Orthop. Res. Soc. 28 (2010) 258–264. https://doi.org/10.1002/jor.20970.
[55] V. Glatt, M. Miller, A. Ivkovic, F. Liu, N. Parry, D. Griffin, M. Vrahas, C. Evans, Improved healing of large segmental defects in the rat femur by reverse dynamization in the presence of bone morphogenetic protein-2, J. Bone Joint Surg. Am. 94 (2012) 2063–2073. https://doi.org/10.2106/JBJS.K.01604.
[56] S.R. Angle, K. Sena, D.R. Sumner, W.W. Virkus, A.S. Virdi, Healing of rat femoral segmental defect with bone morphogenetic protein-2: a dose response study, J. Musculoskelet. Neuronal Interact. 12 (2012) 28–37.
[57] L.E. Rustom, T. Boudou, S. Lou, I. Pignot-Paintrand, B.W. Nemke, Y. Lu, M.D. Markel, C. Picart, A.J. Wagoner Johnson, Micropore-induced capillarity enhances bone distribution in vivo in biphasic calcium phosphate scaffolds, Acta Biomater. 44 (2016) 144–154. https://doi.org/10.1016/j.actbio.2016.08.025.
[58] N. Zwetyenga, S. Catros, A. Emparanza, C. Deminiere, F. Siberchicot, J.-C. Fricain, Mandibular reconstruction using induced membranes with autologous cancellous bone graft and HA-betaTCP: animal model study and preliminary results in patients, Int. J. Oral Maxillofac. Surg. 38 (2009) 1289–1297. https://doi.org/10.1016/j.ijom.2009.07.018.
[59] C. Christou, R.A. Oliver, Y. Yu, W.R. Walsh, The Masquelet technique for membrane induction and the healing of ovine critical sized segmental defects, PloS One. 9 (2014) e114122. https://doi.org/10.1371/journal.pone.0114122.
[60] V. Viateau, M. Bensidhoum, G. Guillemin, H. Petite, D. Hannouche, F. Anagnostou, P. Pélissier, Use of the induced membrane technique for bone tissue engineering purposes: animal studies, Orthop. Clin. North Am. 41 (2010) 49–56; table of contents. https://doi.org/10.1016/j.ocl.2009.07.010.
[61] E. de Monès, S. Schlaubitz, H. Oliveira, J.-M. d'Elbée, R. Bareille, C. Bourget, L. Couraud, J.-C. Fricain, Comparative study of membranes induced by PMMA or silicone in rats, and influence of external radiotherapy, Acta Biomater. 19 (2015) 119–127. https://doi.org/10.1016/j.actbio.2015.03.005.
[62] X. Wang, F. Luo, K. Huang, Z. Xie, Induced membrane technique for the treatment of bone defects due to post-traumatic osteomyelitis, Bone Jt. Res. 5 (2016) 101–105. https://doi.org/10.1302/2046-3758.53.2000487.
[63] R.D. Verboket, M. Leiblein, M. Janko, A. Schaible, J.C. Brune, K. Schröder, M. Heilani, C. Fremdling, Y. Busche, T. Irrle, I. Marzi, C. Nau, D. Henrich, From two stages to one: acceleration of the induced membrane (Masquelet) technique using human acellular dermis for the treatment of non-infectious large bone defects, Eur. J. Trauma Emerg. Surg. Off. Publ. Eur. Trauma Soc. 46 (2020) 317–327. https://doi.org/10.1007/s00068-019-01296-x.
[64] T. Gualdi, R. Laurent, V. Moutarlier, M. Fenelon, A. Nallet, F. Pouthier, L. Obert, B. de Billy, C. Meyer, F. Gindraux, In vitro osteodifferentiation of intact human amniotic membrane is not beneficial in the context of bone repair, Cell Tissue Bank. 20 (2019) 435–446. https://doi.org/10.1007/s10561-019-09778-3.
[65] M. Fénelon, S. Catros, J.C. Fricain, What is the benefit of using amniotic membrane in oral surgery? A comprehensive review of clinical studies, Clin. Oral Investig. 22 (2018) 1881–1891. https://doi.org/10.1007/s00784-018-2457-3.
[66] S. Spinella-Jaegle, S. Roman-Roman, C. Faucheu, F.W. Dunn, S. Kawai, S. Galléa, V. Stiot, A.M. Blanchet, B. Courtois, R. Baron, G. Rawadi, Opposite effects of bone morphogenetic protein-2 and transforming growth factor-beta1 on osteoblast differentiation, Bone. 29 (2001) 323–330.
[67] W. Li, G. Ma, B. Brazile, N. Li, W. Dai, J.R. Butler, A.A. Claude, J.A. Wertheim, J. Liao, B. Wang, Investigating the Potential of Amnion-Based Scaffolds as a Barrier Membrane

for Guided Bone Regeneration, Langmuir ACS J. Surf. Colloids. 31 (2015) 8642–8653. https://doi.org/10.1021/acs.langmuir.5b02362.

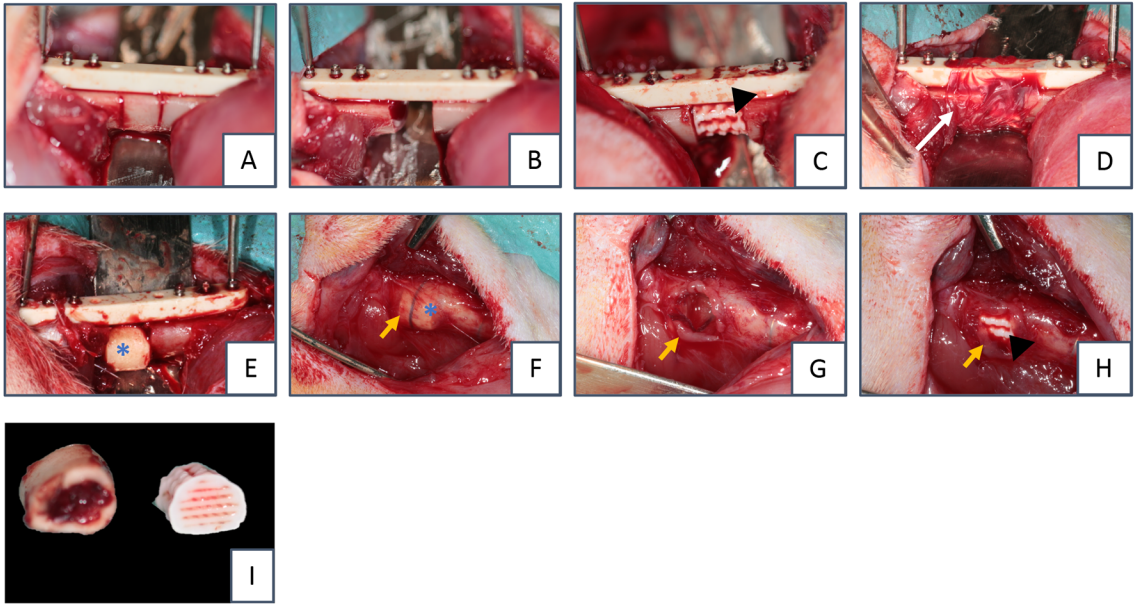
A
B
C
D
E
F
G
H
I

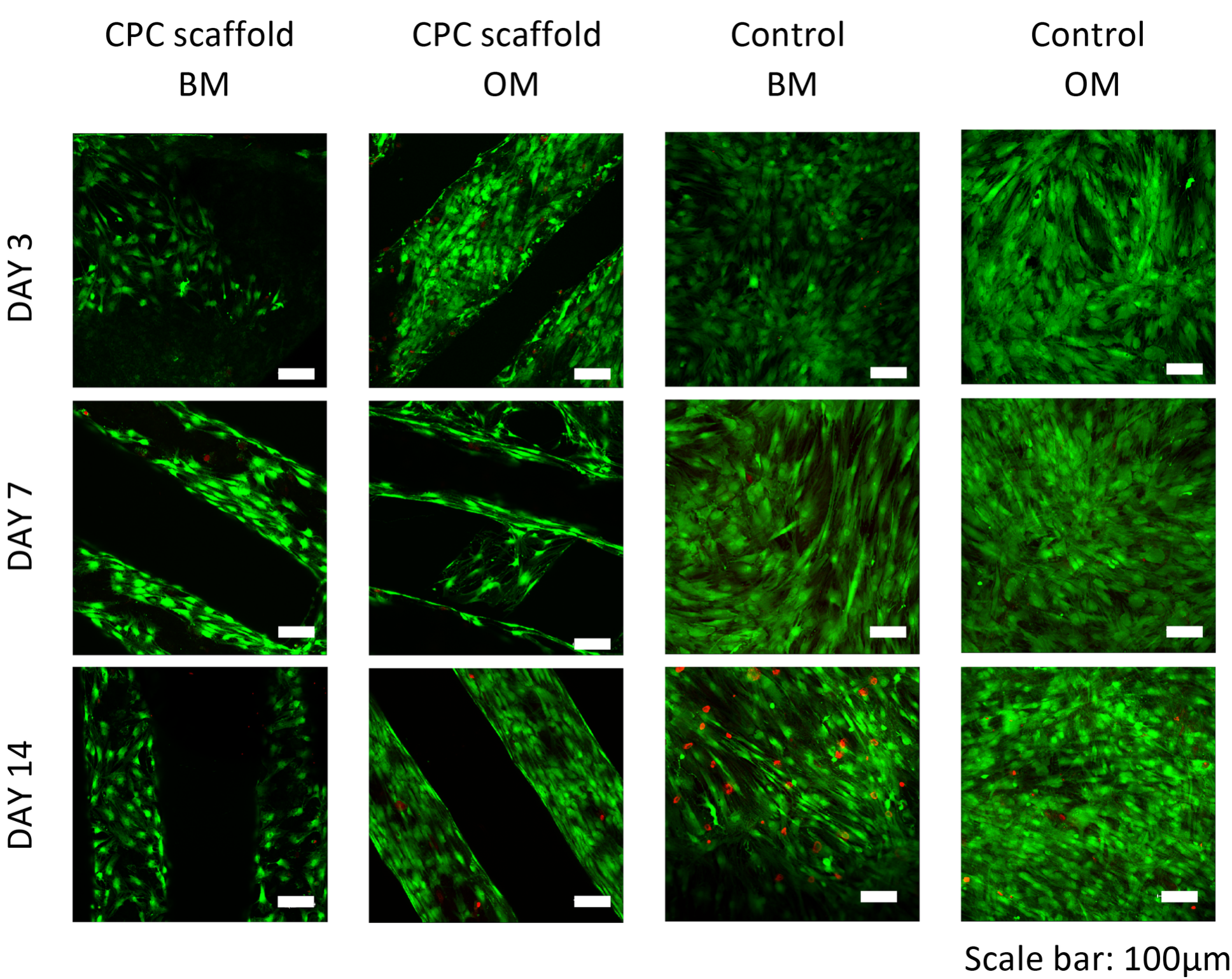
CPC scaffold BM
CPC scaffold OM
Control BM
Control OM
DAY 3
DAY 7
DAY 14
Scale bar: 100µm

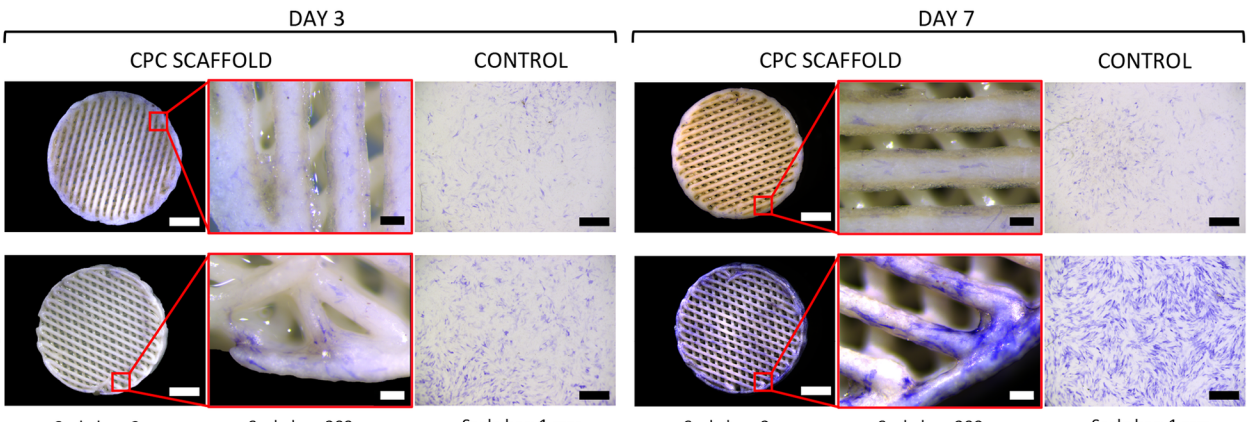
DAY 3
DAY 7
CPC SCAFFOLD
CONTROL
CPC SCAFFOLD
CONTROL
BM
OM
Scale bar: 2mm
Scale bar: 200 µm
Scale bar: 1 mm
Scale bar: 2mm
Scale bar: 200 µm
Scale bar: 1 mm

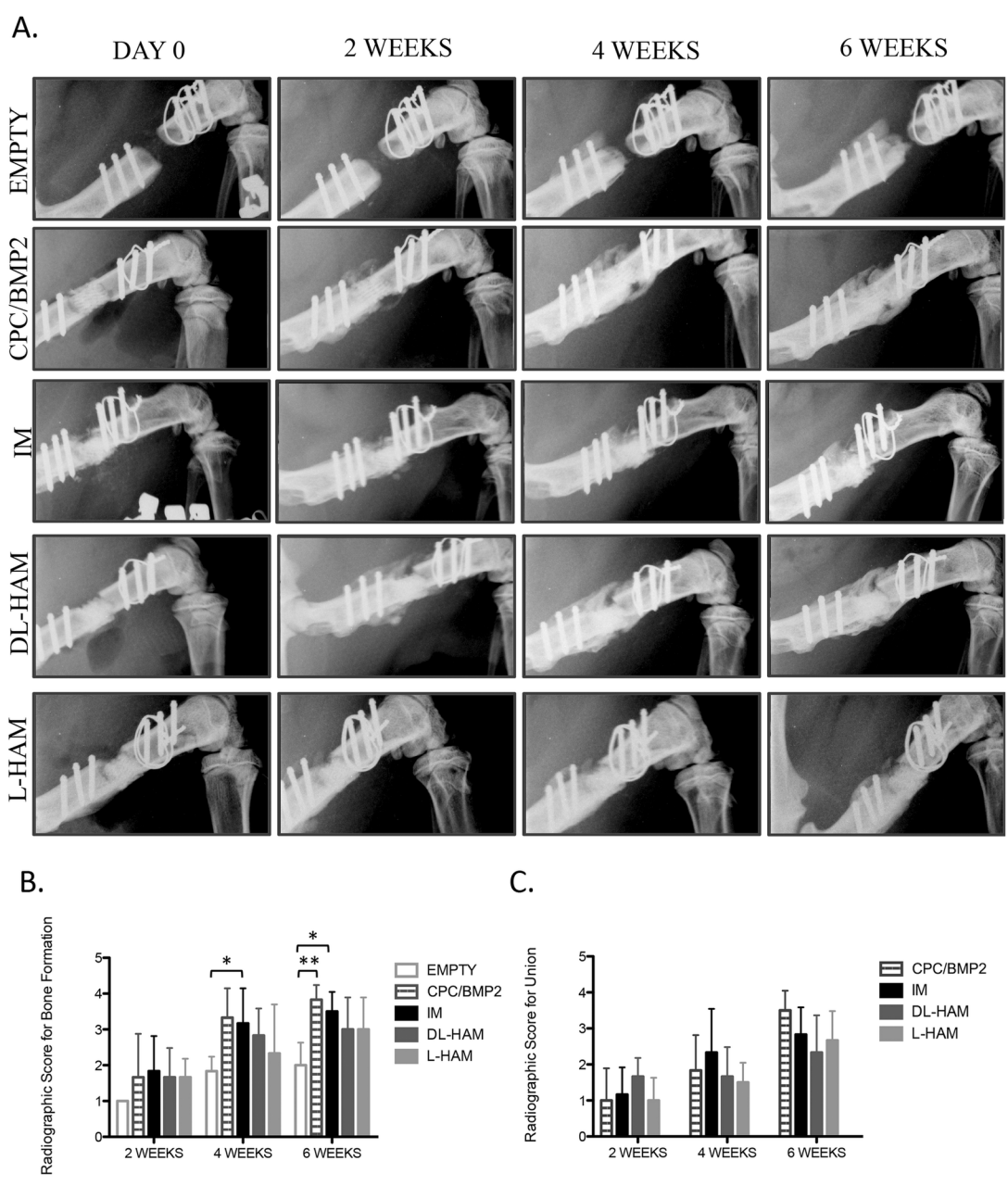
A.
DAY 0
2 WEEKS
4 WEEKS
6 WEEKS
EMPTY
CPC/BMP2
IM
DL-HAM
L-HAM
B.
Radiographic Score for Bone Formation
0
1
2
3
4
5
2 WEEKS
4 WEEKS
6 WEEKS
*
*
**
EMPTY
CPC/BMP2
IM
DL-HAM
L-HAM
C.
Radiographic Score for Union
0
1
2
3
4
5
2 WEEKS
4 WEEKS
6 WEEKS
CPC/BMP2
IM
DL-HAM
L-HAM

A.

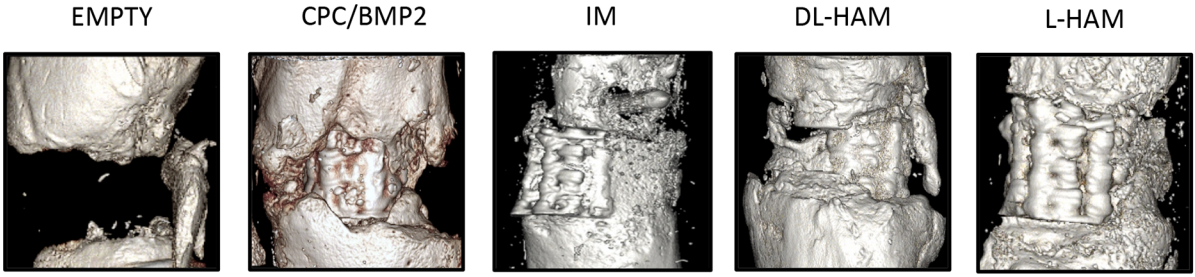
EMPTY
CPC/BMP2
IM
DL-HAM
L-HAM

B.

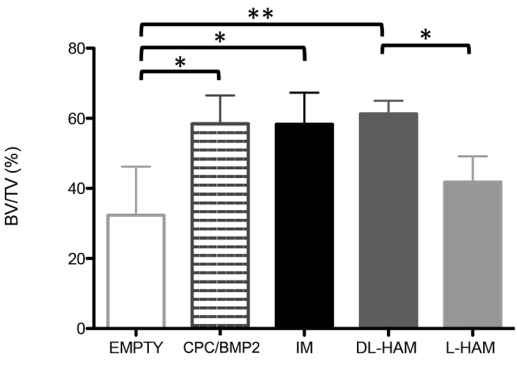
**
*
*
*
80
60
40
20
0
BV/TV (%)
EMPTY
CPC/BMP2
IM
DL-HAM
L-HAM

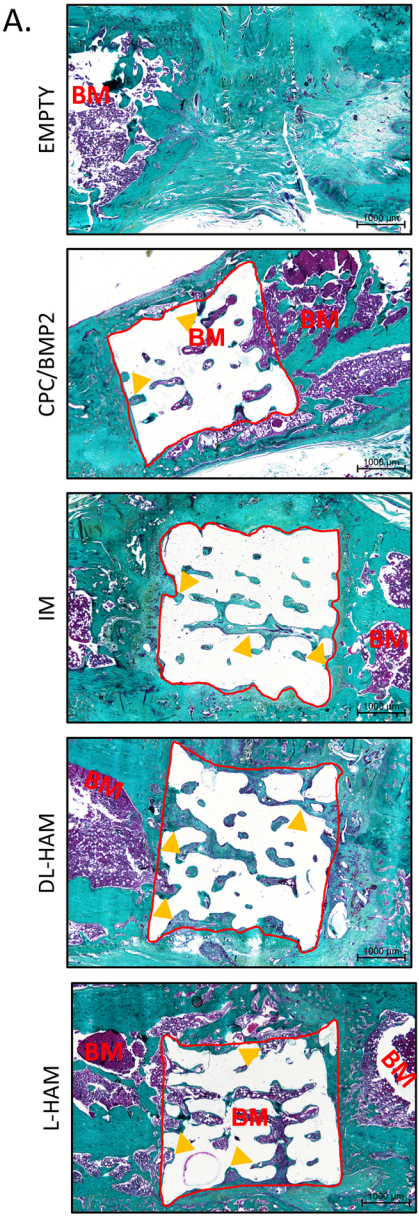
A.
EMPTY
CPC/BMP2
IM
DL-HAM
L-HAM
BM
1000 µm
B.
Bone area in pores (%)
100
80
60
40
20
0
CPC/BMP2
IM
DL-HAM
L-HAM
C.
Hard tissue response at scaffold interface
5
4
3
2
1
0
CPC/BMP2
IM
DL-HAM
L-HAM
D.
Hard tissue response within the pores
*
5
4
3
2
1
0
CPC/BMP2
IM
DL-HAM
L-HAM
E.
Global histological score for tissue response
10
8
6
4
2
0
CPC/BMP2
IM
DL-HAM
L-HAM

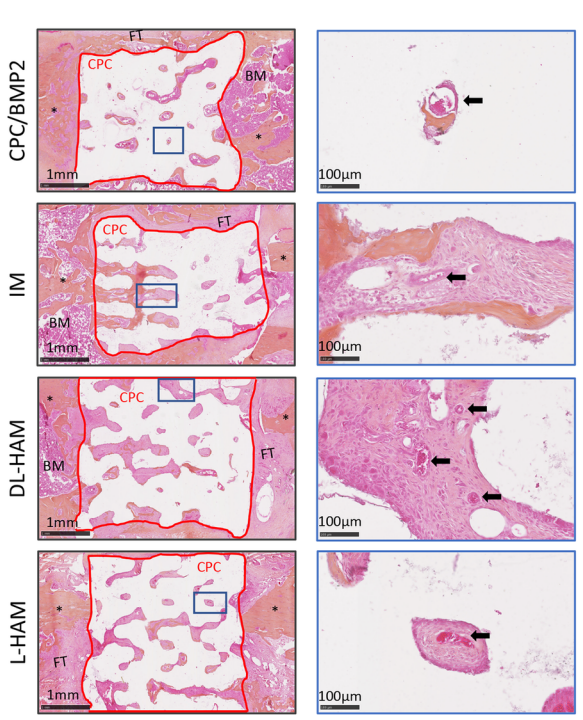
A.
B.
CPC/BMP2
IM
DL-HAM
L-HAM
CPC
FT
BM
1mm
100µm

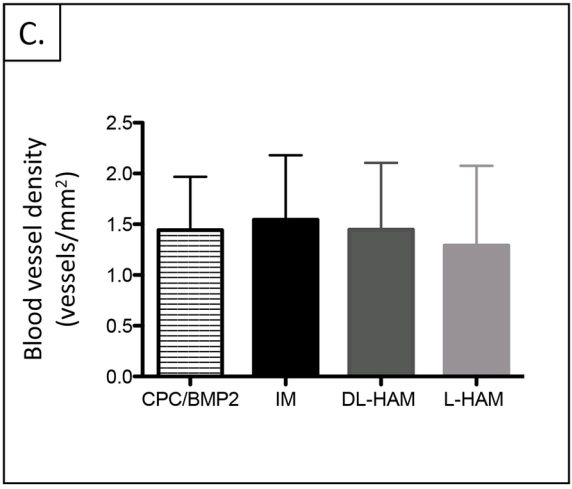
C.
Blood vessel density (vessels/mm²)
2.5
2.0
1.5
1.0
0.5
0.0
CPC/BMP2
IM
DL-HAM
L-HAM

Group	Name	Defect Fillings
1	EMPTY	Left empty
2	CCP/BMP2	CPC scaffold + rhBMP-2
3	L-HAM	CPC scaffold + rhBMP-2 covered by L-HAM
4	DL-HAM	CPC scaffold + rhBMP-2 covered by DL-HAM
5	IM	CPC scaffold + rhBMP-2 covered by the induced membarne

Hard tissue response at scaffolf interface	Score
Direct bone to implant contact without soft interlayer	4
Remodeling lacuna with osteoblasts and/or osteoclasts at surface	3
Majority of implant is surrounded by fibrous tissue capsule	2
Unorganized fibrous tissue (majority of tissue is not arranged as a capsule)	1
Inflammation marked by an abundance of inflammatory cells and poorly organized tissue	0

Hard tissue response within the pores	Score
Tissue in pores is mostly bone	4
Tissue in pores consists of some bone within mature, dense fibrous tissue and/or few inflammatory response elements	3
Tissue in pores is mostly immature fibrous tissue (with or without bone) with blood vessels and young fibroblasts invading the space and few macrophagespresent	2
Tissue in pores consists mostly of inflammatory cells and connective tissue components in between (with or without bone) or the majority of the pores areempty or filled with fluid	1
Tissue in pores is dense and exclusively of inflammatory type (no bone present)	0

Presence of cartilage tissue formation	Score
Yes	1
No	0

INDUCED MEMBRANE

1st surgery

Resection + stabilization

Cement spacer

2nd surgery

Spacer removal
+ 3D printed CPC scaffold

AMNIOTIC MEMBRANE

1 surgery

Resection + stabilization

L- HAM
or DL-HAM

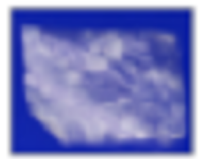

3D-PRINTED
CPC SCAFFOLD

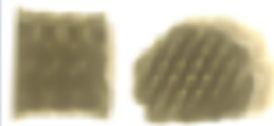

BONE REGENERATION ?

LONGITUDINAL
PLANAR X-RAYS

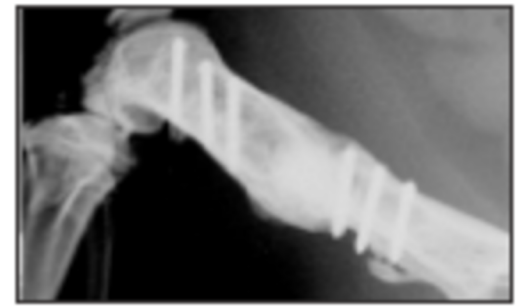

MICRO-CT
ANALYSIS

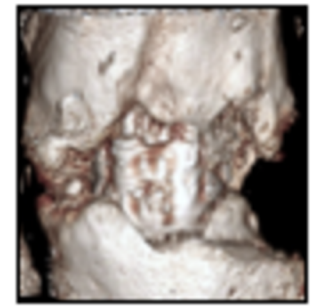

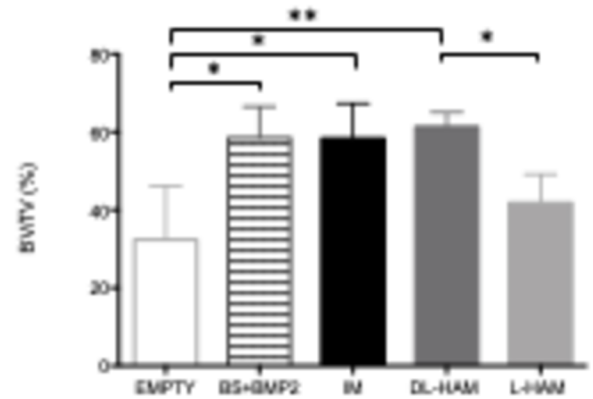

HISTOLOGICAL ANALYSIS